Closed-Loop Analysis of Manual Flare and Landing

Robert K. Heffley*
Systems Technology, Inc., Mountain View, Calif.

An approach to analyzing the manual flare and landing of an airplane is described here. The basis of this approach is a mathematical model of the flare maneuver which is derived from manual landings of both real and simulated aircraft. This flare model, in turn, lends itself to a linear closed-loop system description of the combined pilot/vehicle. Furthermore, simple Laplace transform methods can be used to map flare performance as functions of the flare maneuver. Having this link between flare maneuver and landing performance, we can estimate the pilot's ease in achieving desired levels of landing performance. Examples of this approach will be given using the results of a STOL airplane approach and landing simulation.

Introduction

THE manual flare and landing task has long been viewed as an open-loop control situation, at least by those trying to treat it analytically. This has resulted in flare models which involve, for example, some specified normal acceleration function or control time history. On the other other hand, most pilots insist that there is a substantial closed-loop aspect to the flare maneuver.

What is offered here is a more direct modeling of the flare maneuver which is based on the heads-up visual information that is available to a pilot during flare. The manner employed in describing the flare maneuver model lends itself to formulation in terms of a closed-loop control system. Then, for the purpose of illustration, this model is combined with a simplified description of the airplane dynamics which, in turn, provides an approach to relating the flare maneuver to landing performance. Analysis techniques involve no more than a linear single-loop control system. This is sufficient, however, to address virtually all the considerations involved in the longitudinal aspects of manual flare and landing.

This paper originated in a joint FAA/NASA STOL simulation program, which is described in Ref. 1. The analytical approach described here was successful in explaining many of the effects on landing caused by variations in approach speed, wind conditions, and pilots.

We will begin by developing the pilot/vehicle model. The model consists of the flare maneuver, the airframe, and certain simplifying assumptions regarding inner control loops. This will lead to a discussion of the dynamics of the flare and speculation on how a pilot arrives at a particular numerical description of his flare. Having done so we can address criteria required for good landing characteristics. Finally, we present an example of how the flare and landing can be analyzed for a particular aircraft.

Flare Model Structure

The flare model presented here is inferred from the data gathered from actual and simulated landings in which the pilot used visual runway information to flare the airplane. The basis of the inference made is the correlation between a control and likely controlled variables.

A plot of attitude vs altitude during flare provides a strong clue to how a closed-loop control structure can be formed. Figure 1 gives an example of some typical manual flares performed on a simulator. This profile suggests the flare maneuver can be approximated by a linear relationship between the altitude variable and the attitude control. With initial conditions: altitude, $h=h_{FL}$; vertical velocity, $\dot{h}=\dot{h}_0$; airspeed, $V=V_0$; and attitude, $\theta=\theta_0$; the pilot begins his flare by pitching the airplane proportionally to decreasing altitude until, at touchdown, $\theta=\theta_0+\Delta\theta$, as shown in Fig. 2. Thus, for the flare (i.e., $h<h_{FL}$) the block diagram shown in Fig. 3 can be constructed.

This model characterizes a large number of examples of landings gathered from both simulator and actual flight results. Furthermore, although this model was originally based on STOL aircraft data, it appears equally applicable to conventional airplanes. A few examples of varied aircraft types are shown in Fig. 4.

So far, we have characterized only the flare maneuver as linear. The description of airplane dynamics may range from a sophisticated nonlinear model to a relatively simple linearized model. For the purposes of this paper the latter will be used to show the effects of the more influential system parameters. If ground effect were significant or angle of attack excursions excessive then a more complex model might be required.†

A particularly useful approximate airframe model for analysis of flare and landing consists of two degrees of freedom (perturbed airspeed, u, and vertical velocity $\dot{h}$), with an attitude control θ_c. This may be expressed as

$$\frac{d}{dt}\begin{bmatrix} u \\ \dot{h} \end{bmatrix} \doteq \begin{bmatrix} X_u & -X_w \\ -Z_u & Z_w^\dagger \end{bmatrix}\begin{bmatrix} u \\ \dot{h} \end{bmatrix} + \begin{bmatrix} X_\alpha - g \\ -Z_\alpha^\dagger \end{bmatrix}\begin{bmatrix} \theta_c \end{bmatrix} \quad (1)$$

where X_u, X_w, Z_u, and $Z_w^\dagger$ are conventional x- and z- force dimensional derivatives taken with respect to x and z velocities in a body fixed stability axis system, $X_\alpha \triangleq V_0 X_w$

$$Z_w^\dagger = \frac{1}{V_0} Z_\alpha^\dagger \triangleq Z_w\left[1 - \frac{M_w}{Z_w}\frac{Z_{\delta_e}}{M\delta_e}\right] \text{(i.e., trimmed } Z_w) \quad (2)$$

and

flight path angle γ_0 is assumed small (3)

This model presumes an altitude control which is much quicker than the desired flight path control. The resulting

Presented as Paper 74-834 at the AIAA Mechanics and Flight Conference, Anaheim, Calif., August 5-9, 1974; Submitted August 21, 1974; revision received April 16, 1975. Based on work performed under Contract NAS2-7926, a joint FAA/NASA program.

Index categories: Aircraft Handling, Stability, and Control; Aircraft Landing Dynamics.

*Senior Research Engineer. Member AIAA.

†Even in some cases, however, ground effect can be adequately approximated with linear stability derivatives taken with respect to altitude (i.e., X_h and Z_h), thus retaining the level of simplification illustrated in this paper.

block diagram using the linear flare maneuver and the dynamic model just given is shown in Fig. 5, where

$$\left[s+\frac{1}{T_{\theta_1}}\right]\left[s+\frac{1}{T_{\theta_2}}\right]=s^2-(Z_w^{\dagger}+X_u)s+Z_w^{\dagger}X_u-X_wZ_u \tag{4}$$

$$\left[s+\frac{1}{T_{h_1}}\right]\doteq s-X_u+Z_u\frac{(X_\alpha-g)}{Z_\alpha^{\dagger}} \tag{5}$$

The airplane dynamics of the above block diagram can also be expressed in terms of transfer function numerators, i.e.

$$h/\theta_c=N_{\delta_e}^{\dot{h}}/sN_{\delta_e}^{\theta}$$

Reference 5 provides detailed background for use of numerators and Ref. 1 uses them in connection with flare and landing analysis.

To recap briefly, we have inferred a pilot model for the flare based on the observation that the attitude control is approximately proportional to altitude. We noted that this model is perfectly usable with a complicated airframe model, but that, in many instances, linearized dynamics suffice. Finally, we defined a simple closed-loop pilot/vehicle system. Our next step will be to use this simplified model to examine the essential features of the flare dynamics.

Dynamics of Flare

Starting with the simple block diagram shown previously, we can proceed to express the fundamental relationships involved in the flare. These relationships consist of the closed-loop response of sink rate, angle of attack, airspeed, and position along the runway.

As indicated earlier, the aircraft model can be described with any level of sophistication desired. The same applies to longitudinal stability augmentation, control systems, and inner-loop closures involving the pilot. However, to illustrate the closed-loop flare model concept we will retain the simplified two-degree-of-freedom model described previously.

Referring back to the linear block diagram we see that the parameters describing the flare consist of: gain $\Delta\theta/h_{FL}$ and amplitude h_{FL} (or $\Delta\theta$). The values of these parameters are set by the pilot during his learning phase for a particular airplane and flight condition. This was observed directly in simulator training sessions. In fact, a strong indicator of learning level for the landing was the consistency of θ vs h profiles. The possible factors which combine to set these flare parameters for the pilot will be discussed shortly.

The flare gain $\Delta\theta/h_{FL}$ determines the denominator of the closed-loop flare transfer functions

$$\Delta=s\left[s+\frac{1}{T_{\theta_1}}\right]\left[s+\frac{1}{T_{\theta_2}}\right]-\frac{\Delta\theta}{h_{FL}}Z_\alpha^{\dagger}\left[s+\frac{1}{T_{h_1}}\right] \tag{6}$$

$$=\left[s+\frac{1}{T_{FL}}\right]\left[s^2+2\zeta_{FL}\omega_{FL}s+\omega_{FL}{}^2\right] \tag{7}$$

where

$$\frac{1}{T_{FL}}\doteq\left[-\frac{\Delta\theta}{h_{FL}}Z_\alpha^{\dagger}\Big/\left(\frac{1}{T_{\theta_1}}\frac{1}{T_{\theta_2}}-\frac{\Delta\theta}{h_{FL}}Z_\alpha^{\dagger}\right)\right]\times\frac{1}{T_{h_1}}\doteq\frac{1}{T_{h_1}} \tag{8}$$

$$\omega_{FL}{}^2\doteq\frac{-\Delta\theta}{h_{FL}}Z_\alpha^{\dagger}+\frac{1}{T_{\theta_1}}\cdot\frac{1}{T_{\theta_2}} \tag{9}$$

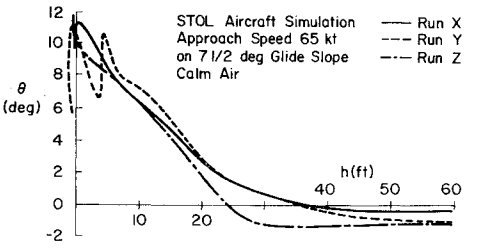

Fig. 1 Typical manual flare profiles.

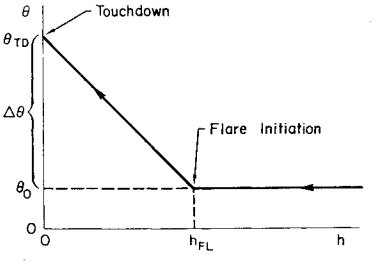

Fig. 2 Inferred manual flare maneuver.

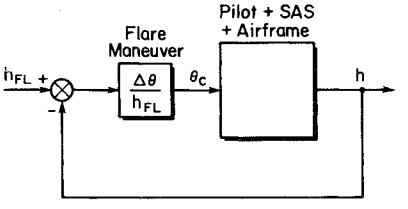

Fig. 3 Block diagram of inferred flare maneuver.

In physical terms the mode at $1/T_{FL}$ corresponds to the flight path divergence (if negative) associated with the backside of the $\dot{h}$ vs V curve. Since this is usually a long time constant compared with the duration of the flare, it can be neglected. The oscillatory mode represents the dominant flare path change. The frequency ω_{FL} describes the abruptness of flare, and the damping ζ_{FL} describes the oscillatory tendency (i.e., ballooning).

Given the closed-loop flare gain $\Delta\theta/h_{FL}$ we can compute the flare trajectory, including touchdown conditions. The following are simplified linear system solutions using inverse Laplace transforms‡ evaluated at the time of touchdown, $t=t_{TD}$

[Flare height]

$$h_{FL}=\mathcal{L}^{-1}\frac{-\dot{h}_0\left[\frac{1}{T_{\theta_1}}\right]\left[\frac{1}{T_{\theta_2}}\right]}{(0)\left[\frac{1}{T_{FL}}\right][\zeta_{FL},\omega_{FL}]} \tag{11}$$

[Touchdown sink rate]

$$\dot{h}_{TD}=\mathcal{L}^{-1}\frac{\dot{h}_0\left[\frac{1}{T_{\theta_1}}\right]\left[\frac{1}{T_{\theta_2}}\right]}{\left[\frac{1}{T_{FL}}\right][\zeta_{FL},\omega_{FL}]} \tag{12}$$

[Touchdown airspeed]

$$V_{TD}=V_0+\mathcal{L}^{-1}\frac{-\dot{h}_0\frac{\Delta\theta}{h_{FL}}\left\{X_\alpha-g\right\}\left[\frac{1}{T_{u_1}}\right]}{(0)\left[\frac{1}{T_{FL}}\right][\zeta_{FL},\omega_{FL}]} \tag{13}$$

‡The following shorthand notation is used here: $[1/T]\triangleq s+1/T$ and $[\zeta,\omega]\triangleq s^2+2\zeta\omega s+\omega^2$.

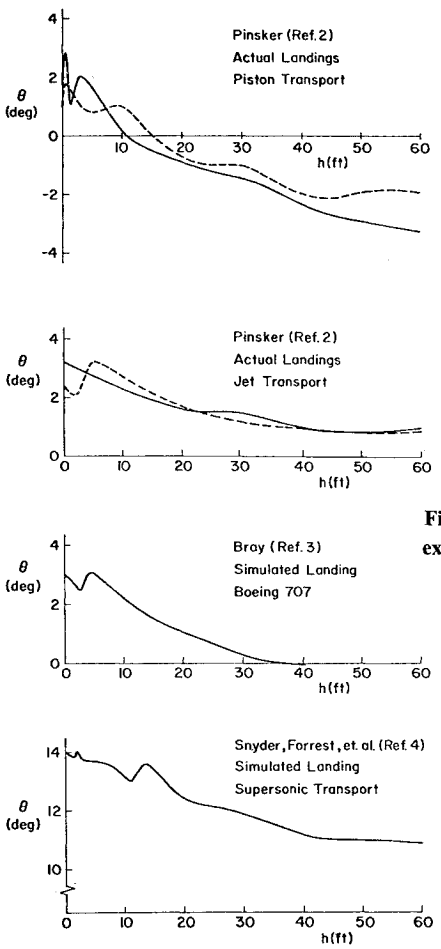

Fig. 4 Flare maneuver examples.

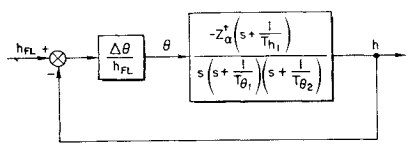

Fig. 5 Block diagram of linear flare model.

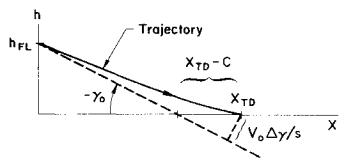

Fig. 6 Derivation of touchdown point relationship.

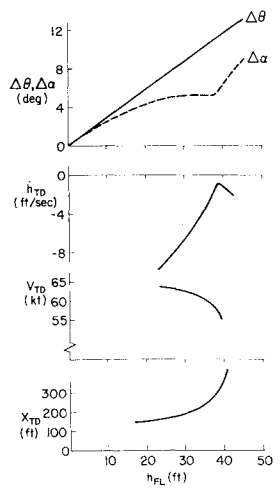

Fig. 7 Landing touchdown conditions for varying flare height, $\Delta\theta/h_{FL}=0.005$ rad/ft.

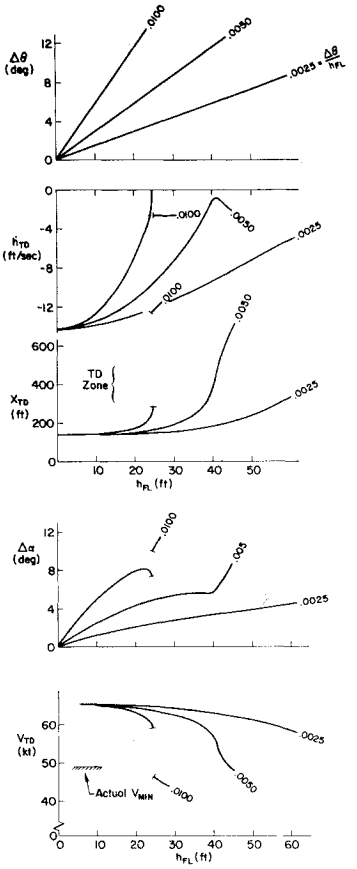

Fig. 8 Landing touchdown conditions for varying flare height and flare gain.

[Touchdown angle of attack]

$$\alpha_{TD}=\alpha_0+\mathcal{L}^{-1}\frac{-\dot{h}_0\dfrac{\Delta\theta}{h_{FL}}\left[\zeta_w,\omega_w\right]}{(0)\left[\dfrac{1}{T_{FL}}\right]\left[\zeta_{FL},\omega_{FL}\right]} \tag{14}$$

where

$$\omega_w^2\doteq-(g/V_0)Z_u \tag{15}$$

and

$$2\zeta_w\omega_w\doteq-X_u \tag{16}$$

[Touchdown point on runway]

$$x_{TD}=C-\mathcal{L}^{-1}V_0\frac{\Delta\theta}{h_{FL}}Z_\alpha^\dagger\frac{\left[\dfrac{1}{T_{\gamma_1}}\right]}{(0)^2\left[\dfrac{1}{T_{FL}}\right]\left[\zeta_{FL},\omega_{FL}\right]} \tag{17}$$

where

$$C=x_{TD}\text{ without a flare} \tag{18}$$

and

$$\frac{1}{T_{\gamma_1}}=-X_u+Z_u\frac{(X_\alpha-g)}{Z_\alpha^\dagger}\doteq\frac{1}{T_{h_1}} \tag{19}$$

This relation can be derived using the sketch in Fig. 6, i.e.

$$x_{TD}-C=(V_0\Delta\gamma/s)/-\sin\gamma_0$$

An example application of the above is shown in Fig. 7 for a typical STOL[§] flare gain of $\Delta\theta/h_{FL}=0.005$ rad/ft. However, instead of plotting the variables vs t_{TD} they are plotted vs h_{FL} to avoid the less important time aspect. The main features of Fig. 7 are the following: 1) Flare below a certain h_{FL} results in a hard landing. 2) If the h_{FL} is too high, an undershoot tendency exists with a larger and rapidly building angle of attack. This is also the point at which speed rapidly bleeds off. 3) The allowable range of h_{FL} to meet given $\dot{h}_{TD}$ and x_{TD} constraints can be readily evaluated.

Note that the plots in Fig. 7 can also be interpreted as trajectories. For example, the plot of $\dot{h}_{TD}$ vs h_{FL} can also be viewed as $\dot{h}(t)$ vs $h_{FL}-h(t)$.

A second variable is added to Fig. 8. Here we see the effect of both gain $\Delta\theta/h_{FL}$ and amplitude h_{FL}. This illustrates the strong effect of high gain on floating and ballooning if the flare is a little too high. (The discontinuity in the lines indicates the part of the trajectory where ballooning occurs.) On the other hand, too low a gain results in hard landings unless the flare is started high.

An $\dot{h}$ plot, such as in Fig. 8, shows the extent to which the maneuver can be considered an exponential flare. Some automatic landing schemes use a control law consisting of $\dot{h}_c=-c_0-c_1\dot{h}$. This provides an exponential decrease of sink rate with respect to time. Consider the $\dot{h}_{TD}$ vs h_{FL} plot in Fig. 8 as $\dot{h}(t)$ vs $h_{FL}-h(t)$. We see that the trajectories resemble straight lines as the airplane closes with the ground if we exclude the cases of ballooning. Hence, the flare maneuver described here will generally resemble an exponential flare.

The goodness of the simple linear analysis is shown in Fig. 9. Here, the $\Delta\theta/h_{FL}=0.005$ case is compared to the conditions calculated, using the actual nonlinear simulator model with an analog pilot performing the nominal flare maneuver. The comparison is good up to the point of floating, which is adequate for the purposes of our analysis.

Pilot Adjustment of Flare Parameters

The ideas presented to this point allow us now to consider the pilot's rationale in choosing his flare parameters (gain and amplitude). This will, in turn, set the stage for setting forth criteria by which to judge the acceptability of flare characteristics for a particular airplane and flight condition.

The upper limit of usable flare gains is set by the tendency to float, if flared just a little too high or to hit hard if flared a little too low. Stated another way, only a relatively small range of flare altitudes result in an acceptable landing if the gain is too high. Figure 8 illustrates the high sensitivity of touchdown sink rate to flare height at high gains.

A low flare gain results in a slow flare maneuver for which there may be inadequate regulation against disturbances. This is clear if we regard the flare gain $\Delta\theta/h_{FL}$ as providing a particular crossover frequency in the altitude control loop. As with any servo control, the crossover frequency determines how quickly disturbances may be countered. In the case of the flare, if the crossover frequency is too low (i.e., the flare too gently) then the aircraft is prone to be carried by gusts. Therefore, a lower bound on pilot gain can be based on disturbance regulation. Flare hight would appear to be set such that an appropriate touchdown sink rate results from the nominal flare gain.

There are other considerations to complicate the choice of flare parameters. Visibility is an important one. Since the flare parameters $\Delta\theta/h_{FL}$ and h_{FL} are totally visual, heads-up relationships, the pilot must be able to judge both of them from flare initiation to touchdown. The most limiting factor is the nose-up attitude at which the pilot loses sight of the runway; thus losing both height and attitude cues. This is more of a problem in a simulator, where there is no visibility to the side that can serve as an alternative to visibility over the nose; therefore, a $\Delta\theta$ limit enters the flare parameter tradeoff problem.

Runway touchdown point is a highly important factor, especially with STOL aircraft. This, then, should be considered in the tradeoff leading to a choice of flare parameters. However, ballooning is almost synonymous with long landings. Thus avoidance of the former takes care of the latter. Short landings are an important limiting factor and are avoided mainly by keeping the flare height high enough.

Another constraint viewed by the pilot is the angle of attack margin from stall during his flare. This translates into how much flare control he has remaining to cope with disturbances. Specific requirements on angle of attack margin are probably difficult for the pilot to formulate without having considerable experience with a particular case involving a range of adverse factors. Other factors, no doubt, exist when optimizing a flare technique. However, based on simulator observations, those mentioned are the most important.

Figure 10 shows an example of the relationship of flare parameters to landing characteristics for an example STOL aircraft. The boundaries shown are defined by specific numerical values depending upon the pilot's criteria for a successful landing.

Criteria for Good Landing Characteristics

In the light of what has just been discussed, the factors which determine an easy-to-land airplane are straightforward: About an easily repeated range of flare parameters, the resulting range of touchdown conditions must be acceptable.

As an example, let's say the pilot can easily start a flare at 35 ± 5 ft and end with an attitude excursion of $10\pm2°$ consistently. If this range of flare gains and amplitude results in touchdowns within specified limits of sink rate and distance along the runway in the presence of expected disturbances, then we would conclude that the airplane has good landing qualities. If, on the other hand, hard, short landings or long, floating landings can occur, then the airplane will be rated poorly.

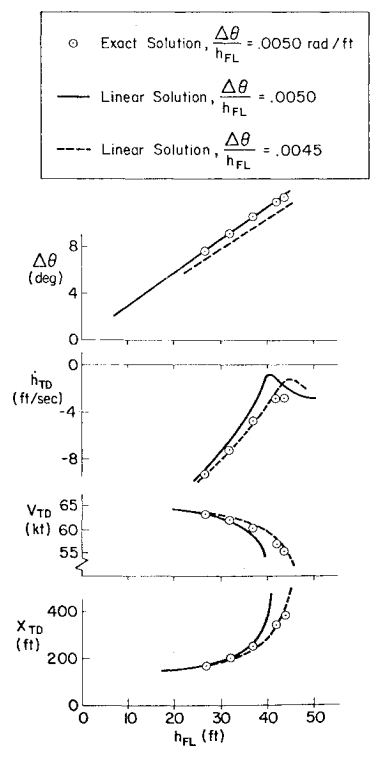

Fig. 9 Comparison of linear airframe solution to exact solution.

§This example is a basic configuration from Ref. 1. The essential parameters required for the analysis presented here are: $V_0=65$ knots,
$\gamma_0=-7.5°$, $Z_\alpha^\dagger=-53.7$ ft/sec^2, $X_\alpha=14.9$ ft/sec^2,
$1/T_{\theta_1}=0.20$ rad/sec, $1/T_{\theta_2}=0.36$ rad/sec, $1/T_{h_1}=0.012$ rad/sec,
$1/T_{\gamma_1}=-0.028$ rad/sec, $1/T_{u_1}^*=0.89$ rad/sec.

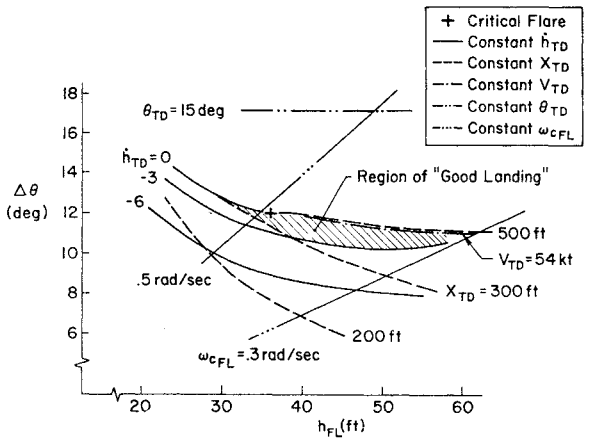

Fig. 10 Touchdown performance vs flare parameters $\Delta\theta$ and h_{FL}; V_0 = 65 knots; $\gamma_0 = -7.5°$ zero mean wind.

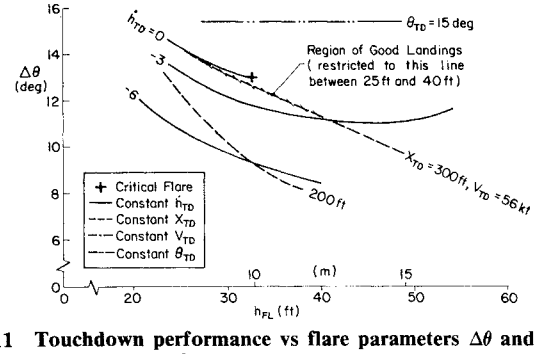

Fig. 11 Touchdown performance vs flare parameters $\Delta\theta$ and h_{FL}; V_0 = 60 knots; $\gamma_0 = -7.5°$, zero mean wind.

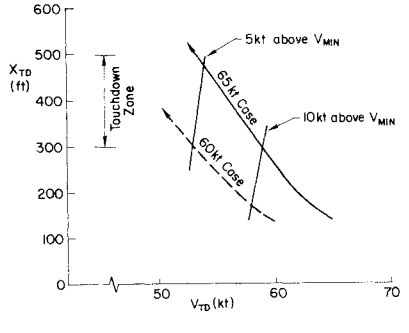

Fig. 12 Touchdown point vs touchdown airspeed for varying approach speed.

The important point here is that the closed-loop analysis of the flare as presented here allows us to begin to describe the success of landing a particular airplane and to pinpoint the qualities which make it good or bad.

Factors Involved in Flare and Landing

Based on the relationships developed to describe the flare maneuver and the characteristics important to the pilot, we can set forth a summary of some of the important quantities involved. At the same time we will define some relationships which prove useful in analyzing the data obtained in experiments.

Flare Gain, $\Delta\theta/h_{FL}$

Flare gain is the commanded attitude relative to altitude during the flare. The desired value is probably established in the pilot's learning phase. The magnitude has a strong effect on closed loop bandwidth of the flare maneuver, i.e., how quickly disturbances may be compensated for. The parameter can be measured directly from a θ vs h history.

Flare Amplitude, h_{FL}

Flare amplitude is the effective altitude at which the flare is begun. It is also determined in the pilot's learning phase. h_{FL}, combined with $\Delta\theta/h_{FL}$, determines mean touchdown conditions. This parameter can also be measured directly.

Attitude Numerator Roots $1/T_{\theta_1}$ and $1/T_{\theta_2}$

Altitude numerator roots are determined primarily by the four stability derivatives X_u, X_w, Z_u, and $Z^{\dagger}_{w}$. The combination of these strongly determines the closed-loop bandwidth obtainable without ballooning.

Sensitivity of Flight Path to Attitude $Z^{\dagger}_{\alpha}$

Sensitivity of flight path to attitude is the product of heave damping $Z^{\dagger}_{w}$ and airspeed. $Z^{\dagger}_{\alpha}$ is the controlled element gain in the flare feedback loop.

Sensitivity of flight path to attitude is the product of heave damping $Z^{\dagger}_{w}$ and airspeed. $Z^{\dagger}_{\alpha}$ is the controlled element gain in the flare feedback loop.

Closed-Loop Natural Frequency in Flare ω_{FL}

Closed-loop natural frequency in flare is the result of closing the flare loop with gain $\Delta\theta/h_{FL}$. This indicates the abruptness of "turning the corner" during flare and is some indication of bandwidth

$$\omega_{FL}^2 \doteq -(\Delta\theta/h_{FL})Z^{\dagger}_{\alpha} + 1/T_{\theta_1} \cdot 1/T_{\theta_2} \tag{20}$$

Closed Loop Flare Bandwidth $\omega_{c_{FL}}$

Closed-loop flare bandwidth is the frequency at which the amplitude of the $h/\theta_c\, j\omega$ bode plot is equal to $(\Delta\theta/h_{FL})^{-1}$

Closed Loop Damping Ratio in Flare ζ_{FL}

Closed-Loop damping ratio in flare is related to the ballooning tendency

$$\zeta_{FL} \doteq \left[\frac{1}{T_{\theta_1}} + \frac{1}{T_{\theta_2}}\right] \Big/ 2\,\omega_{FL} \tag{21}$$

Net Attitude Excursion, $\Delta\theta$

$\Delta\theta$ is a measure of flare maneuver amplitude.

Critical Closed Loop Natural Frequency in Flare, $\omega_{FL_{crit}}$

This is determined by the largest $\Delta\theta/h_{fL}$ for which the airplane does not quite balloon. This appears to be a good approximation to the actual pilot determined flare maneuver.

$$\omega_{FL_{crit}} \doteq \left[5\,\frac{1}{T_{\theta_1}} \quad \frac{1}{T_{\theta_2}}\left(\frac{1}{T_{\theta_1}} + \frac{1}{T_{\theta_2}}\right)\right]^{1/3**} \tag{22}$$

Critical Flare Height, $h_{FL_{crit}}$

This is the height at which the critical flare must be started and appears to correspond to measured flare heights.

$$h_{FL_{crit}} \doteq -\frac{\pi}{2}\,\frac{\dot{h}_0}{\omega_{FL_{crit}}} \tag{23}$$

Critical Flare Gain, $\Delta\theta/h_{FL}\,|crit$

This is the gain used in the critical flare.

$$\frac{\Delta\theta}{h_{FL}}\Big|_{crit} \doteq \frac{-\omega^2_{FL_{crit}}}{Z^{\dagger}_{\alpha}} \tag{24}$$

**This is based on the assumption that the overshoot to steady-state ratio of a simple second order system is $.1/\zeta$. This is valid for $.15 < \zeta < .5$.

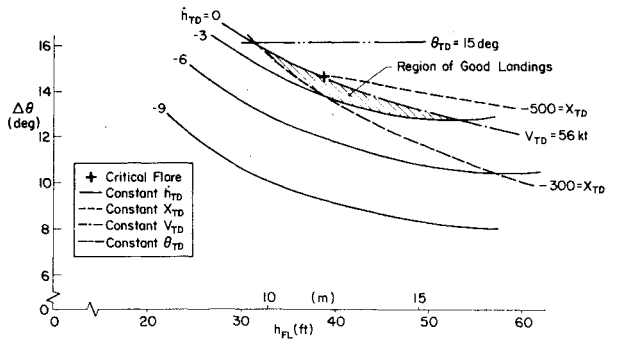

Fig. 13 Touchdown performance vs flare parameters $\Delta\theta$ and h_{FL}; V_θ = 65 knots; 7.5° glide slope, 10-knot tailwind.

Example of Flare and Landing Analysis

The approach developed previously will now be applied to a specific STOL airplane simulator model. The main goal will be to show the general relations between the flare maneuver and the resulting touchdown performance. In particular, we will illustrate the effect of approach speed and the effect of surface winds.

The 65 knot approach case was described previously in Fig. 10. There, we saw that, for various specified touchdown conditions, we could plot the flare required in terms of $\Delta\theta$ and h_{FL}. The regions of particular interest are those in which the conditions prescribed by the piloting task are met. These regions might reasonably consist of: 1) Sink rate at touchdown better than 6 fps and, if possible, better than 3 fps. 2) Touchdown point inside of the marked touchdown zone, 300-500 ft beyond runway threshold. 3) Airspeed at touchdown at some margin above $V_{\min}$ to allow for tailwind gusts, roughly 5 knots. 4) Attitude at touchdown which allows ground visibility over the nose, 15° for this simulation. 5) Closed loop bandwidth to regulate against disturbances, say, 0.3 rad/sec. 6) Some level of dynamic stability in the basic pilot/vehicle flare feedback loop.

For the 65-knot case, Fig. 10 shows a range of flare maneuvers which could meet the requirements. The effect of reducing the approach speed by 5 knots is shown in Fig. 11. While the range of flares which meet the sink rate requirements has actually expanded slightly, we find the touchdown point is much more a problem. In fact, at this speed the airplane reaches the touchdown speed margin of 5 knots (i.e., 5 knots above $V_{\min}$ for approach power setting) at the same time it enters the touchdown zone. Noting the x_{TD} and V_{TD} track one another, Fig. 12 shows this effect of appraoch speed more clearly.

Since this is the product of a linear solution, the low-speed margin results may not be accurate, however, the trend probably remains. That is, for a relatively small change in approach speed the usable touchdown zone can change drastically. Also, we see that there can be an important relation between a particular airplane and the specific runway/glide slope geometry. For example, the runway layout used in this simulation was well suited to this airplane flying a 7.5° glide slope at 65 knots. Desired sink rates and touchdown points were compatible. However, another airplane may require a different distance between glide slope/runway intercept and the touchdown zone for the same compatibility between $\dot{h}_{TD}$ and x_{TD} (and V_{TD}).

Steady wind conditions present a different type of problem. First, a significant adjustment in flare is required for a "good" landing. Second, an adjustment in approach speed is required to offset a loss in margin above $V_{\min}$.

Figure 13 shows a plot of touchdown performance vs flare parameters for a 10-knot tailwind at 65 knots. The approach is flown at a lower power setting, thus an increased pitch attitude. The main difference between this and the zero wind condition is a net shift upward of $\Delta\theta$ for the region of good landings. This amounts to 3° in $\Delta\theta$ and 4° in terms of θ_{TD}. As Fig. 13 shows, this difference could account for a significant difference in both $\dot{h}_{TD}$ and x_{TD}. Also, the same 5 knot margin about $V_{\min}$ (for approach power) is encountered earlier in the touchdown zone.

In view of the approach speed effect shown earlier, it appears that the tailwind effect on speed margin and touchdown zone could be reached without airspeed becoming too low, and touchdown attitudes would be more reasonable.

Extensions of Model

The simplified linear pilot/vehicle model of flare and landing that has been presented can be augmented to account for a number of possible influencing factors.

One feature open to question is the use of a pure gain feedback between h and θ_c. Although a pure gain appeared to fit most examples, forms of pilot compensation such as lead or lag could be considered. To the extent that the pilot uses sink rate in his application of flare control, then lead compensation is appropriate. Most recorded flare profiles, however, indicate that, where compensation deviates from a pure gain, it is generally in the direction of a net lag rather than lead.

Another variation on the simple pure gain attitude flare model is the use of power to flare. Although the use of power to break sink rate is impractical for airplanes having a generally horizontal thrust vector, it may be useful in case of a nearly vertical thrust vector. This can include many powered lift vehicles.

In a recent simulation of STOL aircraft, pilots were requested to try flaring solely with power. In cases where pilots were successful, the profile of throttle vs h was generally similar to the θ vs h cases shown here.

Conclusions

The manual flare and landing of an airplane can be approximated well with a simple linear feedback model. While the flare model can be used with a complex airframe model, it can be combined with a simplified airframe model to point out the essential pilot/vehicle features which influence flare and landing. Several important landing factors, such as sink rate, touchdown point, airspeed loss, and bandwidth, can be plotted as functions of the flare parameters $\Delta\theta$ and h_{FL}. This gives an overall view of potential problems involved in landing a particular aircraft. A particularly important feature of this mapping is the indication of possible incompatibility between glide slope intercept and touchdown zone. The application of this model to an example of a specific STOL airplane reveals a particularly adverse effect of tailwinds on the flare and landing. Finally, this model appears to be of use in dealing with flares using power in place of attitude control.

References

[1] Heffley, R. K., Stapleford, R. L., Rumold, R. C., Lehman, J. M., Hynes, C. S., and Scott, B. C., "A STOL Airworthiness Investigation Using a Simulation of an Augmentor Wing Transport." Vol. II: Simulation Data and Analysis," FAA-RD-74-179, II; NASA TM X-62, 396; STI TR 1047-1, II; Oct. 1974, Systems Technology, Inc., Mountain View, Calif.

[2] Pinsker, W. J. G., "The Landing Flare of Large Transport Aircraft," Aeronautical Research Council, R&M 3602, 1969, Royal Aeronautical Establishment, Bedford, England.

[3] Bray, R. S., "A Piloted Simulator Study of Longitudinal Handling Qualities of Supersonic Transports in the Landing Maneuver," NASA TN D-2251, April 1964.

[4] Snyder, C. T., Fry, E. B., Drinkwater III, F. J., Forrest, R. D., Scott, B. C., and Benefield, T. D., "Motion Simulator Study of Longitudinal Stability Requirements for Large Delta Wing Transport Airplanes during Approach and Landing with Stability Augmentation Systems Failed," NASA TM X-62, Dec. 1972.

[5] McRuer, D., Ashkenas, I., and Graham, D., *Aircraft Dynamics and Automatic Control,* 1st ed., Princeton Univ. Press, Princeton, N.J., 1973.